JOURNAL OF SOLID STATE CHEMISTRY **124,** 366–373 (1996)
ARTICLE NO. 0251

Synthesis, Crystal Structure, Raman Spectroscopy, and Physical Characterization of a New Cobalt Phospho-Silicide $CoSi_3P_3$

H. Vincent,[1] J. Kreisel, Ch. Perrier, O. Chaix-Pluchery, P. Chaudouet, and R. Madar

Laboratoire des Matériaux et du Génie Physique (*CNRS UMR 5628*),
ENS de Physique de Grenoble, 38402 St Martin d'Hères, France

and

F. Genet and G. Lucazeau

Laboratoire d'Electrochimie et Physicochimie des Matériaux et Interfaces (*CNRS UMR 5631*),
ENS d'Electrochimie et d'Electrométallurgie de Grenoble, 38402, St Martin d'Hères, France

Received April 22, 1996; accepted April 25, 1996

New phospho-silicide $CoSi_3P_3$ has been synthesized and its crystal structure determined by single crystal X-ray diffraction ($R = 0.035$, $R_W = 0.042$). $CoSi_3P_3$ ($Z = 4$) crystallizes with the pseudo-orthorhombic symmetry and meriedric twinning in the space group $P2_1$. Lattice parameters are $a = 5.899(1)$ Å, $b = 5.703(1)$ Å, $c = 12.736(1)$ Å, $\beta = 90°$. The crystal structure can be described by zigzag chains of octahedra occupied by Co atoms alternating with zigzag chains of tetrahedra occupied by P or Si atoms. Single crystals of this phase have been investigated at room temperature by polarized Raman spectroscopy in the 100–600 cm^{-1} range. The results confirm the monoclinic symmetry of $CoSi_3P_3$. Magnetic susceptibility and electronic conductivity have been measured between 300 and 10 K. $CoSi_3P_3$ is diamagnetic at room temperature and paramagnetic below 65 K. $CoSi_3P_3$ is semiconducting at room temperature with an energy gap of about 0.12 eV.

INTRODUCTION

A lot of binary metal silicides and phosphides have been prepared and investigated many years ago (1–4). Almost all transition metals give silicides with the formulas M_3Si, M_5Si_3, MSi, and MSi_2. In addition to these four principal compositions, the only other reported examples of silicon-rich phases have formulas Fe_2Si_5 and $IrSi_3$.

Phosphorus is generally used as dopant in Si based IC technology. Since transition metal silicides are now widely used as contacts in VLSI technology, it is of great interest to get a better knowledge of the ternary phases which may result from the interaction of these compounds with a phosphorus doped silicon. Few ternary systems of silicon–phosphorus–transition metals have been studied. Folberth and Pfister (5) prepared and studied $CuSi_2P_3$ which is isostructural with ordered chalcopyrite. Vogel and Giessen (6) studied the iron–phosphorus–silicon phase diagram and quoted the existence of the $FeSi_4P_4$ compound. II'Nitskaya and Kuz'ma studied the Ni–Si–P system (7) and determined the crystal structure of $Ni_{1.68}Si_{0.88}P_3$ and $NiSi_3P_4$ (7, 8). No other phases containing transition metals were reported when we decided to synthesize and characterize such ternary compounds. We have already reported the synthesis and crystal structure of new metal phospho-silicides MSi_xP_y with M = Fe, Co, Ni, Ru, Pd, Os, Ir, Pt (9, 10). A detailed study of compounds MSi_4P_4 (M = Fe, Ru, Os) (11) and MSi_3P_3 (M = Rh, Ir) (12, 13) has been published. Recently, Jeitschko and colloborators began a systematic study of the same ternary phospho-silicides; ordered sphalerite-like structure has been proposed for the $Ni_{1.28}Si_{1.28}P_3$ (or $NiSi_2P_3$) compound (14). In the present paper a new member of the phospho-silicide family rich in nonmetallic atoms (silicon and phosphorus) is presented: $CoSi_3P_3$.

SYNTHESIS

Two to five millimeter large crystals of $CoSi_3P_3$ have been synthesized by flux technique, using tin as the solvent material as mentioned in previous papers (11, 12). Prepared crystals often had tridimensional shape; sometimes platelets with faces perpendicular to the c axis were obtained. The absence of tin in the crystals and their exact chemical composition were checked by microprobe analysis.

Powder samples were obtained by heating mixtures of highly pure element sealed in evacuated silica tubes at

[1] To whom correspondence should be addressed.

0022-4596/96 $18.00

TABLE 1
Crystallographic Data and Data Collection Parameters for $CoSi_3P_3$

Chemical formula	$CoSi_3P_3$	$CoSi_3P_3$
Crystal system	monoclinic	orthorhombic
Space group	$P2_1$	$P2_12_12_1$
Cell parameters		
a (Å)	5.899(1)	
b (Å)	5.703(1)	
c (Å)	12.736(2)	
β (°)	90.00(1)	
Volume (Å^3)	428.5	
Z	4	
ρ calc (g/cm^{-3})	3.66	
Crystal size (mm)	$0.20 \times 0.18 \times 0.16$	
Color	shiny black	
Radiation	Mo$K\alpha$ (λ = 0.71073 Å) graphite monochromated	
μ(Mo$K\alpha$) (cm^{-1})	58.0	
Scan mode	ω	
Scan width	1.40°	
Range measured	$3° \le 2\theta \le 80°$ $-10 \le h \le 10$ $0 \le k \le 10$ $-23 \le l \le 23$	
Period of intensity control	100 reflections	
Measured reflections	5640	
Independent reflections	2825	2651
Internal consistency factor	0.036	0.041
Observed reflections ($I > 3\sigma(I)$)	2545	2346
Parameters refined	140	62
Weighting scheme	$w^{-1}(F^2) = \sigma^2(F^2) + (0.04F^2)^2$	$w^{-1}(F) = \sigma^2(F) + 0.02F^2$
Residuals	R = 0.035, R_W = 0.042	R = 0.067, R_W = 0.082

1250°C for 2 weeks, as described before (11, 12). The reaction product was identified by X-ray diffraction patterns using a Guinier camera and Cr$K\alpha_1$ radiation.

CRYSTAL STRUCTURE

1. Experimental

Precession photographs taken at room temperature show the apparent crystal symmetry to be orthorhombic. The reflections $0k0$ with $k = 2n + 1$ are systematically absent indicating the presence of 2_1 screw-axis along the b direction. According to this preliminary study, the likely space group was $P22_12$. However, $h00$ and $00l$ reflections with h or $l = 2n + 1$ were absent or very weak indicating the presence of pseudo-2_1 screw-axis along the other principal directions; in this case the most probable space groups were $P2_12_12_1$ or, better, considering a monoclinic cell with $\beta = 90°$, $P2_1$ space group in which $h00$ and $00l$ reflections with h or $l = 2n + 1$ are authorized. An X-ray powder pattern could be indexed on the basis of the observed orthorhombic cell.

A prismatic crystal fragment of dimensions about $0.21 \times 0.18 \times 0.16$ mm was mounted on a Nicolet P3 four-circle diffractometer. Cell parameters refined from Bragg angles of 25 accurately measured reflections are given in Table 1. Reflections (5640) have been collected in half the Ewald sphere ($\theta \le 40°$); details about the data collection are summarized in Table 1.

2. Structure Determination

For structure solution and full matrix least squares refinement the software packages SDP (15) and SHELX (16) were used. In a first step, attempts were carried out to describe the crystal structure in orthorhombic space groups. Reflections were averaged in the orthorhombic 222 Laue class. Using the statistical methods of Wilson with any symmetry center excluded, an attempt was made to solve the structure in the $P22_12$ group, but unsuccessfully. Crystal structure was then solved in the $P2_12_12_1$ space group by direct method and Fourier difference analysis. Further on, absorption effects were empirically corrected by using the DIFABS program (17). The distribution of silicon and phosphorus atoms on the nonmetallic sites was found by population refinement.

Results of this first study were not very satisfactory: R and R_W agreement factors were mediocre, 0.068 and 0.082,

TABLE 2
Atomic Parameters of $CoSi_3P_3$ in the $P2_1$ Space Group

Atom	x	y	z	U_{eq} (Å^2)[a]
Co1	0.0062(1)	0.4660(1)	0.12115(5)	0.0061(1)
Co2	0.5180(1)	0.0335(1)	0.38540(6)	0.0063(1)
Si1	0.8287(3)	0.4698(4)	0.6806(1)	0.0079(3)
Si2	0.3720(3)	0.4341(4)	0.7775(2)	0.0084(3)
Si3	0.0797(3)	0.8337(4)	0.0462(1)	0.0075(3)
Si4	0.4714(3)	0.4022(3)	0.3282(1)	0.0077(3)
Si5	0.9359(3)	0.5010(3)	0.4277(1)	0.0077(3)
Si6	0.3627(3)	0.4147(3)	0.0723(1)	0.0080(3)
P1	0.9732(3)	0.0889(3)	0.1741(1)	0.0073(2)
P2	0.4391(3)	0.0175(3)	0.0724(1)	0.0074(2)
P3	0.8761(3)	0.1069(3)	0.4266(1)	0.0076(2)
P4	0.3485(3)	0.0413(3)	0.8200(1)	0.0070(2)
P5	0.8693(3)	0.0760(3)	0.7191(1)	0.0070(2)
P6	0.5872(3)	0.6613(3)	0.4502(1)	0.0074(3)

[a] $U_{eq} = \frac{1}{3} \Sigma_{i \le j} \vec{a_i} \cdot \vec{a_j} / a_i \cdot a_j) \cdot U_{ij}$. $\vec{a_i}$ and $\vec{a_j}$ are unit cell vectors.

respectively, and the distribution of P and Si atoms was not clearly defined on two sites. We refined the crystal structure in the $P2_1$ space group, that is a subgroup of $P2_12_12_1$. The 4*a* position (x, y, z) in $P2_12_12_1$ gives, after $c/4$ origin translation, two 2*a* positions, (x, y, $z - \frac{1}{4}$) and ($x + \frac{1}{2}$, $-y + \frac{1}{2}$, $-z - \frac{1}{4}$). This refinement did not give the best results; crystallographic and weighted factors did not improve $R = 0.061$ and $R_W = 0.081$, and P and Si atom distribution on nonmetallic sites was not clearly established. The lattice symmetry being higher than the space group symmetry, a meriedric twinning has been considered. A last refinement including four twinned domains of comparable volume gave much better results: agreement factors were $R = 0.035$ and $R_W = 0.042$, and P and Si atoms were completely ordered on nonmetallic sites. Figure 1 represents the twinning model. According to the monoclinic symmetry, hkl and $-hk-l$ reflections are equivalent; then domains (1) and (2) on the one hand, and domains (3) and (4) on the other hand, have the same structure factors. Details about crystal structure refinement in $P2_1$ are given in Table 1. Table 2 gives atomic parameters and Table 3 observed interatomic distances. A view along the *a* axis of the crystal structure is presented in Fig. 2. Listings of the structure factors and anisotropic thermal parameters are available from the authors.

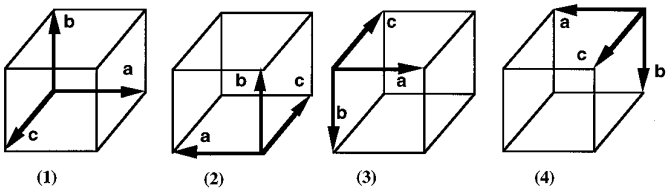

FIG. 1. Twining model proposed for $CoSi_3P_3$.

3. Crystal Structure Description

The two metallic atoms Co1 and Co2 are surrounded by six nearest nonmetallic neighbors, three silicon and three phosphorus atoms distributed at the vertices of an octahedron as in $FeSi_4P_4$ (11). In contrast to $FeSi_4P_4$ or $RhSi_3P_3$ structures in which the metal octahedra are isolated, each Co1 octahedron is linked by two Si3 corners to two Co1 octahedra forming an infinite zigzag chain along the *b* axis direction. In the same way, Co2 octahedra linked by P6 vertices form infinite zigzag chains along the same direction. The two chains are separate. The shortest Co–Co distances in each chain are Co1–Co1 = 4.203 Å and Co2–Co2 = 4.086 Å; between neighboring chains the shortest one is Co1–Co2 = 5.069 Å. In each octahedron Co atom is off-center located; distances Co–Si3 or Co–P6, i.e., distances Co–common corner of two octahedra, are longer than the others, as in ionic compounds because of the electronic repulsion (2.32 compared to about 2.24 Å).

Each P or Si atom is surrounded by four nearest neighbors located at vertices of a tetrahedron. Most tetrahedra have one (or two) Co atoms located at vertices and overlap with one (or two) octahedron, while one corner (or two) of these tetrahedra is located on center of one (or two) octahedron. However two atoms, i.e., P2 and Si5, are completely surrounded by nonmetallic atoms; P2 has four Si neighbors and Si5 four P neighbors. Each P2 tetrahedron is linked by two Si6 corners to two P2 tetrahedra, forming an infinite zigzag chain along the *b* axis direction. In the same way, Si5 tetrahedra linked by P3 vertices form infinite zigzag chains along the same direction. Both chains have no common corner and stand apart from each other. Like in $FeSi_4P_4$, the P–Si mean distance observed in the P2 tetrahedron (2.305 Å) is larger than the Si–P distance found in the Si5 tetrahedron (2.256 Å). The tetrahedron enclosing P atom is slightly larger than the tetrahedron enclosing Si, as expected.

The Co1 and Co2 octahedra separate chains are connected to each other by P2 and Si5 tetrahedra chains. Each P2 tetrahedron connects by corners one Co1 chain with another Co1 chain and with one Co2 chain; in the same way, each Si5 tetrahedron connects between them two Co2 and one Co1 chains. In the two P2 and Si5 tetrahedra, the fourth corner is linked to one vertex of a second octahedron of the same chain obtained from the first one by 2_1 symmetry axis. In this way each P2 or Si5 tetrahedron connects by corners two Co octahedra of the same chain with two Co octahedra belonging to two other chains. Similarly each Co octahedron connects together by corners four tetrahedron chains: Co1 links three P2 and one Si5 chains, and Co2 links three Si5 and one P2 chains. In $CoSi_3P_3$ as in $FeSi_4P_4$ there are neither Si–Si nor P–P links, only Si–P links; Si–P distances are comparable in both structures (from 2.24 to 2.34 Å).

TABLE 3
Bond Lengths and Angles in $CoSi_3P_3$

Co1	Distance	Angle				
Si6	2.212(2)					
P5	2.251(2)	88.92(8)				
P1	2.262(2)	92.29(8)	91.36(7)			
P4	2.263(2)	175.39(8)	87.11(6)	90.14(8)		
Si3	2.317(2)	84.59(8)	173.21(8)	86.90(8)	99.45(7)	
Si3	2.345(3)	80.08(8)	93.34(8)	170.95(8)	97.81(8)	87.54(5)
	Co1	Si6	P5	P1	P4	Si3
Co2						
P3	2.216(2)					
Si1	2.240(2)	171.58(8)				
Si4	2.242(2)	90.95(8)	85.33(9)			
Si2	2.246(2)	89.49(8)	82.86(7)	88.40(8)		
P6	2.302(2)	88.95(7)	98.45(8)	88.04(8)	176.09(10)	
P6	2.314(2)	85.44(8)	98.39(9)	176.23(8)	92.67(8)	90.78(5)
	Co2	P3	Si1	Si4	Si2	P6
Si1						
Co2	2.240(2)					
P1	2.291(3)	136.08(11)				
P5	2.311(3)	109.40(10)	93.65(10)			
P3	2.347(3)	113.84(10)	89.60(10)	111.74(11)		
	Si1	Co2	P1	P5		
Si2						
Co2	2.246(2)					
P2	2.262(2)	125.80(11)				
P1	2.303(3)	113.95(10)	97.38(10)			
P4	2.310(3)	118.62(11)	92.01(10)	104.81(11)		
	Si2	Co2	P2	P1		
Si3						
P1	2.273(3)					
Co1	2.317(2)	112.98(11)				
Co1	2.345(3)	103.29(9)	128.72(10)			
P2	2.388(3)	82.15(9)	1007.3(9)	119.97(10)		
	Si3	P1	Co1	Co1		
Si4						
Co2	2.242(2)					
P6	2.250(3)	110.76(9)				
P4	2.307(3)	122.13(11)	101.50(11)			
P5	2.320(3)	126.24(11)	99.33(10)	92.23(9)		
	Si4	Co2	P6	P4		
Si5						
P5	2.236(3)					
P3	2.244(3)	112.75(10)				
P6	2.268(3)	119.59(11)	103.60(10)			
P3	2.275(3)	105.27(11)	110.35(10)	104.96(11)		
	Si5	P5	P3	P6		
Si6						
Co1	2.212(2)					
P2	2.260(3)	133.39(11)				
P4	2.303(3)	119.61(10)	91.26(10)			
P2	2.310(3)	108.33(10)	98.88(10)	99.35(10)		
	Si6	Co1	P2	P4		
P1						
Co1	2.262(2)					
Si3	2.273(3)	111.81(9)				
Si1	2.291(3)	118.60(10)	104.37(11)			
Si2	2.303(3)	121.33(10)	101.00(11)	96.94(9)		
	P1	Co1	Si3	Si1		
P2						
Si6	2.260(3)					
Si2	2.262(2)	112.32(10)				
Si6	2.310(3)	110.75(10)	107.64(11)			
Si3	2.388(3)	103.35(10)	117.59(11)	104.91(10)		
	P2	Si6	Si2	Si6		
P3						
Co2	2.216(2)					
Si5	2.244(3)	128.00(10)				
Si5	2.275(3)	109.62(10)	100.61(9)			
Si1	2.347(3)	120.42(10)	91.44(10)	102.58(11)		
	P3	Co2	Si5	Si5		
P4						
Co1	2.263(2)					
Si6	2.303(3)	115.29(9)				
Si4	2.307(3)	129.13(10)	92.25(10)			
Si2	2.310(4)	108.51(10)	113.54(11)	96.52(10)		
	P4	Co1	Si6	Si4		
P5						
Si5	2.236(3)					
Co1	2.251(2)	122.34(10)				
Si1	2.311(3)	93.53(10)	119.77(10)			
Si4	2.320(3)	98.35(9)	113.47(10)	105.66(10)		
	P5	Si5	Co1	Si1		
P6						
Si4	2.250(3)					
Si5	2.268(3)	85.63(10)				
Co2	2.302(2)	109.78(10)	103.38(9)			
Co2	2.314(2)	107.64(9)	119.00(10)	124.52(9)		
	P6	Si4	Si5	Co2		

RAMAN SPECTROSCOPY

1. Experimental

Raman spectra were collected using a Dilor XY multichannel spectrometer, equipped with a microscope. The 514.5 nm line of an Ar ion laser was focused to a 1 μm^2 spot. We have checked that laser power up to 15 mW, measured at the surface of the sample, did not produce significant damage of the sample. Standard experiments have been carried out using an incident power of 7 mW. All measurements, performed under microscope, were recorded in backscattering geometry. The instrumental resolution was $2.8 \pm 0.2\ cm^{-1}$. The samples were platelet shaped single crystals, 10 μm thick, with planes perpendicular to the c axis. The laboratory frame, X, Y, Z axes are taken parallel to the principal axes of the crystal.

2. Band Assignment

In order to check the actual crystal symmetry (orthorhombic or monoclinic), the band assignment has been performed for both $P2_1$ and $P2_12_12_1$ (C_2^2 and D_2^4) possible space groups. The 28 atoms of the primitive cell give rise

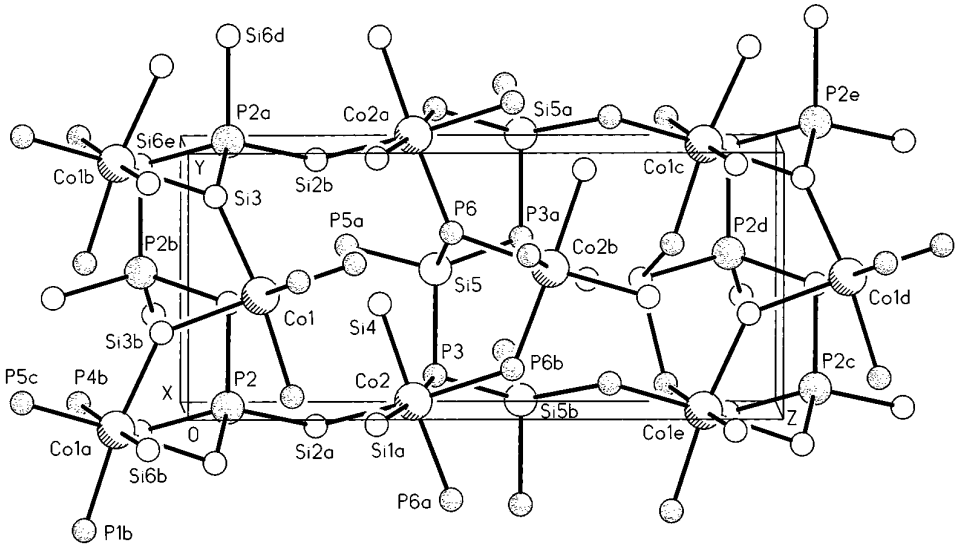

FIG. 2. Crystal structure of $CoSi_3P_3$ viewed along the *a* axis. Co, P2, and Si5 atoms have been enlarged in order to enhance the occupied polyhedra.

to 81 zone center vibrational modes. In the C_2^2 space group, all $(41A + 40B)$ modes are Raman and IR active. In the D_2^4 space group, 60 $(20B_1 + 20B_2 + 20B_3)$ modes are Raman and IR active and 21 *A* modes are Raman active. The platelet shape of the crystals allows only one propagation direction for the laser beam along the *Z* direction, which limits the polarization configurations to $Z(XX)\bar{Z}$, $Z(YY)\bar{Z}$, $Z(XY)\bar{Z}$, and $Z(YX)\bar{Z}$. The $Z(XX)\bar{Z}$ and $Z(YY)\bar{Z}$ geometries allow one to obtain *A* or A_1 modes in the C_2^2 or D_2^4 structure assumption, respectively. The *B* or B_1 modes are similarly obtained from the $Z(XY)\bar{Z}$ and $Z(YX)\bar{Z}$ configurations.

3. Results and Discussion

(a) All Raman spectra obtained in the four polarization configurations show a large polarization effect, some lines disappearing completely by changing the polarization. This indicates that the orientation and the crystalline quality of the sample are well adapted for these experiments. Nevertheless, some unresolved components appear in both the $Z(XX)\bar{Z}$ and $Z(XY)\bar{Z}$ configurations of the crystal. Due to the strong polarization effect observed for the other lines, they have been considered as distinct lines. Thus, 31 bands are observed in the $Z(XX)\bar{Z}$ configuration instead of 41 in the monoclinic or 21 in the orthorhombic structure. The absence of some lines (too weak or masked by stronger lines of the same mode) is compatible with the monoclinic case but a large excess of bands is not acceptable; thus, the orthorhombic structure must be ruled out. This conclusion is strengthened by the observation of 32 bands in the $Z(XY)\bar{Z}$ configuration instead of 40 in the monoclinic assumption or 20 in the orthorhombic one (Fig. 3). The observed frequencies and band assignment are listed in Table 4.

(b) Some *A* modes are shifted in frequency when changing the configuration from $Z(XX)\bar{Z}$ to $Z(YY)\bar{Z}$; see

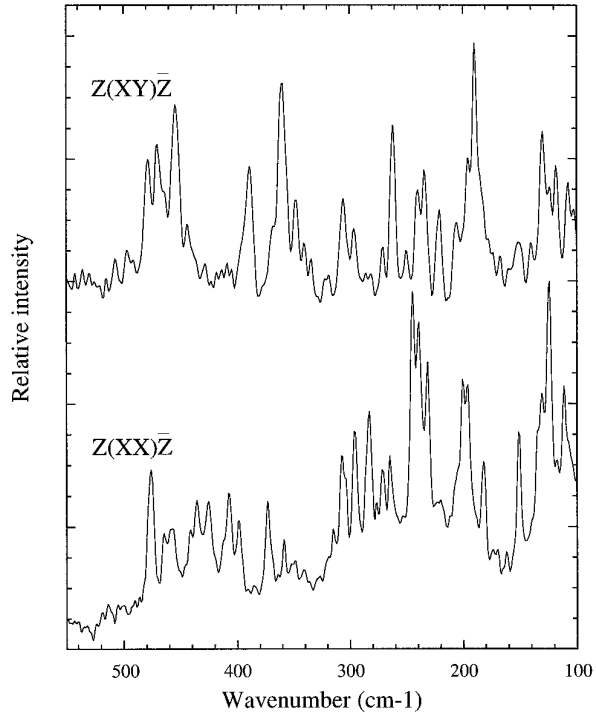

FIG. 3. Polarized Raman spectra of $CoSi_3P_3$; *A* modes and *B* modes are observed in $Z(XX)Z$ and $Z(XY)Z$ configurations, respectively.

TABLE 4
Observed Frequencies and Band Assignment of $CoSi_3P_3$ Raman Modes

Exp. frequencies (cm^{-1})	Mode assignment	Exp. frequencies (cm^{-1})	Mode assignment
107.5	*B*	281.8	*A*
111.3	*A*	296.1	*A*
119.1	*B*	298.0	*B*
123.0	*B*	305.7	*B*
124.1	*A*	307.5	*A*
130.8	*A* and *B*	315.1	*A*
134.7	*A*	322.8	*B*
140.5	*B*	347.4	*B*
150.2	*A* and *B*	358.7	*A*
154.1	*B*	359.5	*B*
181.1	*A*	362.4	*B*
185.0	*B*	371.8	*B*
189.9	*B*	372.7	*A*
196.5	*A* and *B*	390.6	*B*
200.4	*A*	396.4	*A* and *B*
204.2	*A*	425.3	*A*
208.1	*B*	428.2	*A*
221.5	*B*	433.8	*A*
225.4	*B*	441.2	*A*
228.2	*B*	443.2	*B*
231.1	*A*	465.5	*A*
235.9	*A*	469.3	*A* and *B*
238.8	*A*	471.1	*B*
240.7	*B*	474.1	*A*
244.5	*A*	476.6	*A*
250.4	*B*	478.6	*B*
261.8	*B*	480.3	*B*
264.6	*A*	485.9	*A*
271.3	*A*	498.9	*B*

Fig. 4. This effect is reproduced when using very low laser power in order to exclude a thermal effect and has been observed in many independent measurements. These frequency shifts can be attributed to an electro-optical effect, encountered when the modes are both Raman and IR active (18, 19). They depend on the transverse or longitudinal character of the modes.

The phonons observed in $Z(XX)\bar{Z}$ or $Z(YY)\bar{Z}$ backscattering geometry propagate along the Z axis. Under the C_2^2 group assumption, these modes belong to the A species. They give rise to an IR dipole along the Y axis and thus, they are transverse modes. A frequency shift due to the change from transverse to longitudinal character is theoretically only obtained by using the $Y(XX)\bar{Y}$ and $Y(ZZ)\bar{Y}$ configurations. Actually, because of the wide optical aperture of the microscope objective, one measures a TO + LO mixture, the proportion of which can vary when rotating the crystal. Thus, the frequency shift observed for lines between 220 and 250 cm^{-1} when going from $Z(XX)\bar{Z}$ to $Z(YY)\bar{Z}$ is likely to be due to such an effect and attests

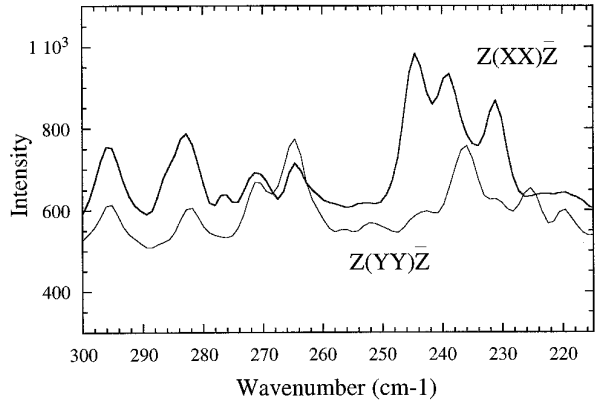

FIG. 4. Polarized Raman spectra of $CoSi_3P_3$ in the range 210–300 cm^{-1}. *A* modes are observed in both $Z(XX)\bar{Z}$ and $Z(YY)\bar{Z}$ configurations.

that the space group is the C_2^2 polar group. This large frequency shift, compared with the other *A* bands (see Fig. 4) indicates that these modes are likely strongly IR active.

PHYSICAL CHARACTERIZATION

1. Electric Resistivity

Electric resistivity of $CoSi_3P_3$ has been measured using single crystals and ceramics between 300 and 80 K. Ceramic disks were prepared by powder sintering at 700–900 K during a week in evacuated silica tubes. Van der Pauw's method was used for measurements of both kinds of sample. Observed energy gaps are similar, and only the initial resistivity values are different because of the resistivity of grain boundaries in the ceramics; see Table 5.

As seen in Fig. 5, $CoSi_3P_3$ is semiconducting with 0.62 Ω cm resistivity and small gap energy, E_a = 0.13(1) eV, at room temperature. Because of the presence of some impurity band, as suggested by the low temperature magnetic susceptibility, apparent E_a decreases with the temperature, E_a = 0.032 eV at 80 K. Between 130 and 180 K the

TABLE 5
$CoSi_3P_3$ Electrical Resistivity Measured on Ceramics and Single Crystal

Sample	ρ (300 K) (Ω cm)	ρ (80 K) (Ω cm)	E_a (300 K) (eV)	E_a (80 K) (eV)
Ceramic sintered at 700°C	48	1563	0.16	0.030
Ceramic sintered at 900°C	44	634	0.14	0.027
Single crystal	0.62	6.3	0.12	0.032

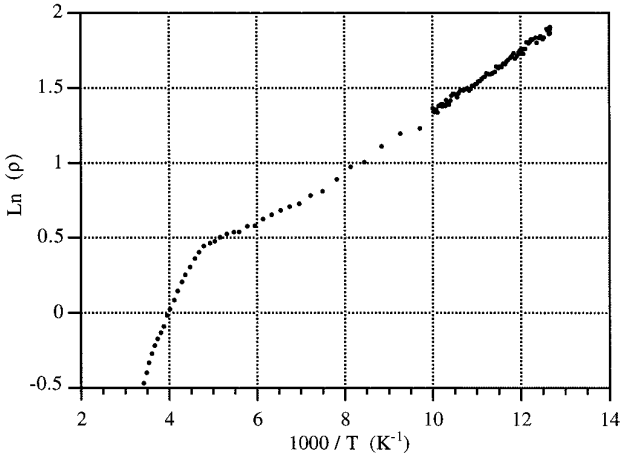

FIG. 5. $CoSi_3P_3$ resistivity measured on platelet crystal.

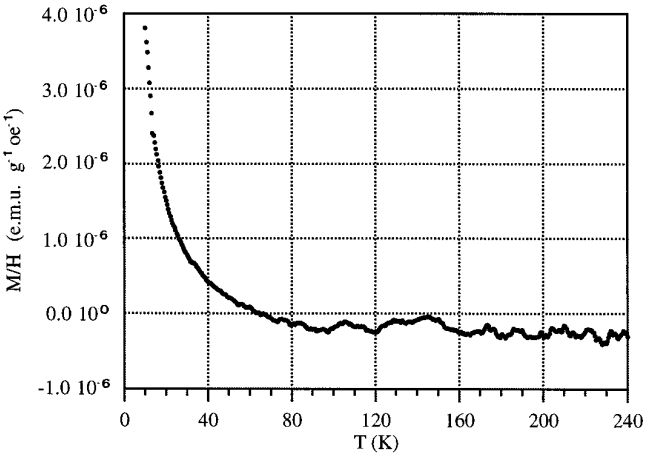

FIG. 7. $CoSi_3P_3$ magnetic susceptibility versus T.

resistivity follows a classical $T^{-3/2}$ law corresponding to a mecanism of electron–phonon diffusion; see Fig. 6.

2. Magnetic Susceptibility

Magnetization measurements have been performed, between 10 and 300 K, on the powder by using a Foner magnetometer. $CoSi_3P_3$ is paramagnetic below 65 K and diamagnetic above. Figure 7 shows $\chi(T)$ after correction of the sample holder contribution; large fluctuations observed at high temperature are due to the addition of fluctuations of both weak signals.

The magnetic susceptibility of a semiconductor is mainly the sum of the lattice and charge carrier susceptibilities: $\chi = \chi_1 + \chi_c$. The χ_1 term results from diamagnetism of the core electrons; its value is temperature independent and can be calculated from tabulated values for different ions (20). Assuming the electronic core configuration of each element is the same as in transition metal silicides, i.e., Me^+ and Si^{2+} (21), and assuming the phosphorus one is P^{5+}, the calculated lattice susceptibility is $\chi_1 = -132 \times 10^{-6}$ emu/mole. In Fig. 8 is plotted observed χ as a function of T^{-1}. Curie law is clearly in evidence below 80 K; the susceptibility straight line is vertically shifted because of the lattice diamagnetic contribution. The χ_1 value estimated from the shift is about -140×10^{-6} emu/mole, in good agreement with the calculated value.

For carriers at low temperature with spin $\frac{1}{2}$, χ_c is given by a Curie law

$$\chi_c = \frac{n\mu_B^2}{k_B T}$$

where n is the carrier concentration, μ_B the Bohr magneton, and k_B the Boltzman constant. At 17 K, the observed Curie susceptibility after correction of the diamagnetic contribution is about $\chi_c = 2.6 \times 10^{-6}$ emu/g; the corre-

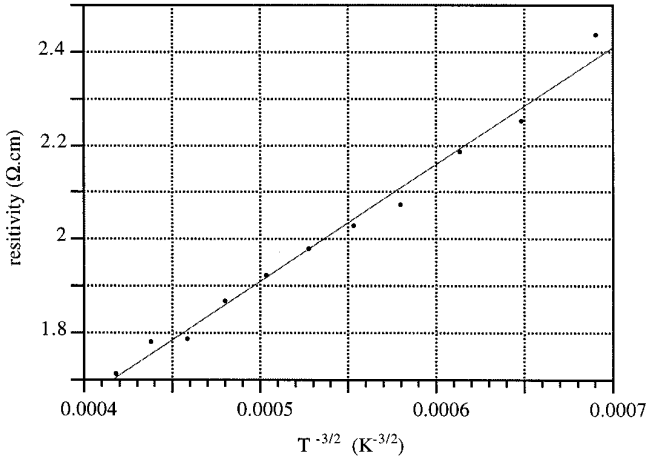

FIG. 6. Low temperature $CoSi_3P_3$ resistivity versus $T^{-3/2}$.

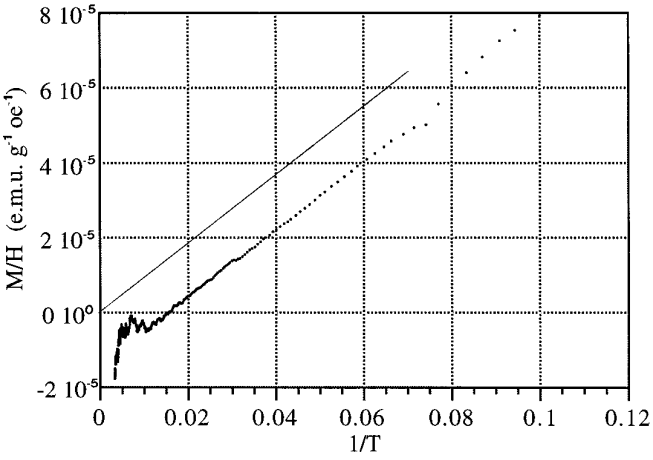

FIG. 8. $CoSi_3P_3$ magnetic susceptibility versus $1/T$.

sponding carrier concentration is $n = 3.2 \times 10^{20}$ by cm^3. On looking at the resistivity value of 0.62 Ω cm measured at room temperature, this n value is rather too high. The high susceptibility χ_c observed at 17 K results probably from a magnetic impurity band localized at low temperature in an isolating state near the conduction band. Deviation from the Curie law observed below 15 K in Fig. 8 can be interpreted as the beginning of random ferromagnetic coupling between impurities.

ACKNOWLEDGMENTS

The authors are grateful to R. Ferré (Laboratoire Louis Néel) and G. Delabouglise for some magnetic and resistivity measurements, and B. Chenevier and U. Gottlieb for helpful discussions.

REFERENCES

1. B. Aronson, T. Lundström, and S. Rundqvist, "Borides, Silicides and Phosphides." Methuen and Co Edt, London, 1965.
2. T. Lundström, *Ark. Kemi.* **31,** 227 (1969).
3. M. Sugitani, N. Kinomura, and M. Koizumi, *J. Solid State Chem.* **26,** 195 (1978).
4. D. J. Braun and W. Jeitschko, *Z. Anorg Allg Chem.* **445,** 157 (1978).
5. O. G. Folberth and H. Pfister, *Acta Crystallogr.* **14,** 325 (1961).
6. R. Vogel and B. Giessen, *Arch. Eisenhüttenw* **30,** 619 (1959).
7. O. N. II'Nitskaya and Yu. B. Kuz'ma, *Zh. Neorg. Khim.* **37**(4), 729 (1992).
8. O. N. II'Nitskaya, V. A. Bruskov, P. Yu. Zavalii, and Yu. B. Kuz'ma, *Izv. Akad. Nauk SSSR, Neorg. Mater.* **27**(6) 1311 (1991).
9. H. Vincent, Ch. Perrier, M. Kirschen, P. Chaudouet, and R. Madar, "11th ICSCTE." Wroclaw, 1994.
10. Ch. Perrier, Thesis, Institut National Polytechnique de Grenoble, 1995.
11. Ch. Perrier, H. Vincent, P. Chaudouet, B. Chenevier, and R. Madar, *Mater. Res. Bull.* **30,** 357 (1995).
12. J. Kreisel, O. Chaix-Pluchery, F. Genet, G. Lucazeau, H. Vincent, and R. Madar, submitted for publication.
13. M. Kirschen, H. Vincent, Ch. Perrier, P. Chaudouet, B. Chenevier, and R. Madar, *Mater. Res. Bull.* **30,** 507 (1995).
14. J. Wallinda and W. Jeitschko, *J. Solid State Chem.* **114,** 476 (1995).
15. B. A. Frenze, "Structure Determination Package." College Station, Texas 77840 (1985).
16. G. Sheldrick, "SHELX93." Institut Anorg. Chemie, D-37077 Göttingen, 1993.
17. N. Walker and D. Stuart, *Acta Crystallogr. Sect. A* **39,** 158 (1983).
18. L. Couture-Mathieu et J.-P. Mathieu, *C. R. Acad. Sci. Paris* **231,** 839 (1950).
19. J.-P. Mathieu et L. Couture-Mathieu, *J. Phys.* **13,** 271 (1952).
20. E. König and G. König, "Magnetic Properties of Coordination and Organometalic Transition Metal Compounds, Landolt-Börnstein" (K. H. Hellwege, Ed.), Vol. II, part 10. Springer-Verlag, Berlin, 1979.
21. U. Gottlieb, A. Sulpice, R. Madar, and O. Laborde, *J. Phys. Condens. Matter* **5,** 8755 (1993).